CO_2 conversion in a gliding arc plasmatron : elucidating the chemistry through kinetic modeling

THE JOURNAL OF PHYSICAL CHEMISTRY C

US University of Sussex

Subscriber access provided by University of Sussex Library

Article

CO Conversion in a Gliding Arc Plasmatron: Elucidating the Chemistry through Kinetic Modelling

Stijn Heijkers, and Annemie Bogaerts

J. Phys. Chem. C, **Just Accepted Manuscript** • DOI: 10.1021/acs.jpcc.7b06524 • Publication Date (Web): 20 Sep 2017

ACS Publications

The Journal of Physical Chemistry C is published by the American Chemical Society. 1155 Sixteenth Street N.W., Washington, DC 20036

CO_2 Conversion in a Gliding Arc Plasmatron: Elucidating the Chemistry through Kinetic Modelling

Stijn Heijkers[1] and Annemie Bogaerts[1*]

[1] Research group PLASMANT, Department of Chemistry, University of Antwerp, Universiteitsplein 1, BE-2610 Wilrijk-Antwerp, Belgium

*annemie.bogaerts@uantwerpen.be, +3232652377

Abstract

By means of chemical kinetics modelling we can elucidate the main dissociation mechanisms of CO_2 in a gliding arc plasmatron (GAP). We obtain good agreement between the calculated and experimental conversions and energy efficiencies, indicating that the model can indeed be used to study the underlying mechanisms. The calculations predict that vibration induced dissociation is the main dissociation mechanism of CO_2, but it occurs mainly from the lowest vibrational levels due to fast thermalization of the vibrational distribution. Based on these findings, we propose ideas for improving the performance of the GAP, but testing these ideas in the simulations reveals that they do not always lead to significant enhancement, due to other side effects, thus illustrating the complexity of the process. Nevertheless, the model allows to obtain more insight in the underlying mechanisms and to identify the limitations.

1. Introduction

The atmospheric CO_2 concentration has been increasing over the last two centuries from approximately 270 ppm to values exceeding 400 ppm, thus accelerating climate change [1].

Significant efforts need to be made to keep the increase in global average temperature well below 2°C, as was agreed at the Paris climate conference (COP21) [2]. Technologies for converting CO_2 into value-added products, such as fuels, are therefore highly desirable, as they can turn waste back into new feedstock, following the cradle-to-cradle principle [3].

In recent years there is increasing interest in using plasmas for CO_2 conversion [4–35]. Besides pure CO_2 splitting into CO and O_2 [5–24], also reactions with CH_4 (i.e., dry reforming) [25–31], H_2O [32], N_2 [33,34] and H_2 [35] are studied. Most research is performed using dielectric barrier discharges (DBDs) [5–7,27–33] and microwave (MW) plasmas [8–16,26,34] . The highest energy efficiencies (> 50% and even up to 90%) have been achieved using a MW-setup, and this is attributed to vibrational excitation, leading to dissociation of CO_2 [11–16]. However, these highest energy efficiencies in MW plasmas were obtained at reduced pressures, which is undesirable for industrial applications. DBDs, on the other hand, operate at atmospheric pressure and they are already used in industry for ozone synthesis [36], but the energy efficiency is more limited (typically up to 10%), since the CO_2 dissociation proceeds mainly through electronic excitation, which is less efficient [16,4]. The conversion and energy efficiency in a DBD can be improved by inserting a packing inside the plasma, but the energy efficiency remains limited [31].

Another type of plasma is recently gaining considerable interest for CO_2 conversion, i.e., the so-called gliding arc (GA) discharge, which operates at atmospheric pressure and is clearly more efficient than the DBD, with values reported around 25-29% [18,19]. A conventional GA discharge is formed between two flat diverging electrodes. The arc ignites at the shortest interelectrode distance and "glides" towards larger interelectrode distance by means of the gas flow, until it extinguishes and a new arc ignites again at the shortest distance, so that the cycle is repeated. However, because of the high current density of the discharge, conventional GA reactors suffer from electrode degradation. Moreover, a

significant amount of gas does not pass through the active plasma (arc) region, so it will not be converted [19,20]. To tackle these issues, a new type of GA discharge, based on cylindrical electrodes and tangential gas inlets, was recently developed. It is also called "gliding arc plasmatron" (GAP), and is based on vortex flow stabilization, i.e. forward vortex flow (FVF) and/or reverse vortex flow (RVF) stabilization [21,37,38]. The highest energy efficiencies for CO_2 conversion were obtained using the RVF configuration, because it is characterized by a secondary, backwards oriented inner vortex gas stream within the outer tangential gas flow, confining the plasma, and resulting in nearly perfect heat insulation from the wall, better gas mixing with the arc, and therefore a higher conversion and energy efficiency [21,23] .

Some experimental work and fluid dynamics modeling have been performed for the GAP, to study the CO_2 conversion under different operating conditions [21,23,25] and to describe the typical gas flow and plasma characteristics in argon [24,38] and in CO_2 [24], respectively. However, to our knowledge, no detailed kinetic study has been performed yet to elucidate the main dissociation mechanisms of CO_2 in a GAP. Nevertheless, this information is crucial to obtain insight in the underlying chemistry in order to improve the process.

Therefore, in this paper we present a detailed study of the CO_2 conversion and energy efficiency in a GAP reactor, using 0D chemical kinetics modeling with a full description of the vibrational kinetics throughout the arc, and validated by experiments. This allows us to elucidate the most important CO_2 dissociation mechanisms, as well as to identify the limitations, which can be helpful to further improve the performance of the GAP for energy efficient CO_2 conversion.

2. Model description

First we will give a general description of the 0D model and the chemistry set used in the simulations, followed by the assumptions in the 0D approach to describe the arc region in the GAP and the conditions used in the model.

2.1 0D Model equations

The 0D model is based on solving a set of conservation equations (1) for all individual species included in the model (see below):

$$\frac{\partial n_s}{\partial t} = \sum_{i=1}^{j}[\left(a_{s,i}^{R} - a_{s,i}^{L}\right)R_i] \quad (1)$$

where n_s is the density of species s (in m^{-3}) , j the total number of reactions, $a_{s,i}^{L}$ and $a_{s,i}^{R}$ the stoichiometric coefficients at the left hand side and right hand side of the reaction and R_i the rate of reaction (in m^{-3} s^{-1}), given by:

$$R_i = k_i \prod_s n_s^{\alpha_{s,i}} \quad (2)$$

where k_i is the rate constant (in m^3 s^{-1} or m^6 s^{-1} for two-body or three-body reactions, respectively). Besides, the balance equation for the gas temperature T_g (in K) is also solved:

$$N\frac{\gamma k}{\gamma - 1}\frac{dT_g}{dt} = P_{e,el} + \sum_j R_j \Delta H_j - P_{ext} \quad (3)$$

where $N = \sum n_i$ is the total neutral species density, γ is the specific heat ratio of the total gas mixture, k is the Boltzmann constant (in J K^{-1}), $P_{e,el}$ is the gas heating power density due to elastic electron-neutral collisions (in W m^{-3}), R_j is the rate of reaction j (in m^{-3} s^{-1}), ΔH_j is the heat released (or consumed when this value is negative) by reaction j (in J) and P_{ext} is the heat loss due to energy exchange with the surroundings (in W m^{-3}). More details about the model can be found in the Supporting Information.

2.2 Chemistry set

The chemistry set used in this study is based on the original model of Kozák et al. [11] which has been thoroughly reviewed by Koelman et al. [39]. The electron impact reaction rate constants are calculated using a pre-evaluated electron energy distribution function (EEDF; which is regularly updated during the simulations based on the new chemical composition in the plasma) and the cross section set of Phelps with the 7 eV threshold excitation reaction used for dissociation [40–42], as suggested by Grovulovic´ et al. [43], Bogaerts et al. [44] and Pietanza et al. [45–47]. The species described in the kinetic model are listed in Table 1.

The symbols 'V' and 'E' between brackets for CO_2, CO and O_2 represent the vibrationally and electronically excited levels of these species, respectively. All 21 levels (V1-V21) of the asymmetric mode till the dissociation limit (5.5 eV) are taken into account, since they are crucial for storing vibrational energy for efficient CO_2 dissociation [16]. In addition, four effective low-lying symmetric stretching and bending mode levels are included in the model (Va-Vd). We only take one electronically excited level (E1) into account with an energy of 10.5 eV, as the excitation level with energy of 7 eV will immediately give rise to dissociation (see above).

A large number of reactions are taken into account, such as electron impact reactions, electron-ion recombination reactions, ion-ion, ion-neutral and neutral-neutral reactions, as well as vibration-translation (VT) and vibration-vibration (VV) relaxation reactions. Furthermore, reactions considering carbon production are also included in the model. More information about the species and reactions included in the model can be found in the papers of Kozák et al. [11], Koelman et al. [39] and Bogaerts et al. [44]

Table 1: Species taken into account in the 0D model.

Molecules	Charged species	Radicals	Excited species
CO_2, CO	CO_2^+, CO_4^+, CO^+, $C_2O_2^+$, $C_2O_3^+$, $C_2O_4^+$, C_2^+, C^+, CO_3^-, CO_4^-	C_2O, C, C_2	CO_2(Va, Vb, Vc, Vd), CO_2(V1-V21), CO_2(E1), CO(V1-V10), CO(E1-E4)
O_2, O_3	O^+, O_2^+, O_4^+, O^-, O_2^-, O_3^-, O_4^-	O	O_2(V1-V3), O_2(E1-E2)
	electrons		

2.3 Modeling the GAP reactor with a 0D approach

The GAP under study is based on the experimental design used by Ramakers et al. [23] and Nunnally et al. [21,22], illustrated in Figure 1. It is a cylindrical GA reactor in which the gas flow enters through a tangential inlet, resulting in a vortex flow. A potential difference is applied between the reactor body and the outlet of the reactor, which act as cathode and anode, respectively. This potential difference creates an arc between the cathode and the anode. When the anode diameter is smaller than the cathode diameter, the incoming gas will not immediately escape the reactor through the outlet at the bottom of the reactor, as it follows a vortex flow with larger diameter, so it will be forced upwards in the cathodic part of the reactor, in a so-called forward vortex flow (FVF) pattern. Due to friction and inertia, the rotational speed will be reduced. Therefore, when the spiraling gas arrives at the top of the reactor, it will start to move downwards in a smaller vortex, towards the outlet at the bottom, i.e., in a reverse vortex flow (RVF). Due to this vortex flow, the arc plasma is stabilized in

the center of the reactor and the reverse vortex gas flow is forced through the plasma. This is schematically illustrated in Figure 1, and described by fluid dynamics modeling by Trenchev et al. [24,38].

The reactor body (or cathode) has a length of 20.3 mm and a diameter of 17.50 mm. Ramakers et al. [23] performed experiments with three grounded electrodes, acting as anode and outlet, with a constant length of 16.30 mm, but different diameters, i.e., 7.08 mm, 14.30 mm and 17.50 mm. In our study, we focus on the anode with the smallest diameter, for which the RVF effect is most pronounced, and therefore it yields the highest conversion and energy efficiency, as explained in [23] .

Combining a complete fluid dynamics and chemical kinetics description of CO_2 conversion in a GAP plasma in a 2D or 3D model is computationally not yet affordable, but since the plasma confined in the inner vortex is more or less uniform [38], we can assume a constant power density applied to the gas, during its residence time in the plasma (i.e., when travelling in the inner (reverse) vortex). Therefore, 0D modeling of this kind of plasma is justified. Indeed, the species conservation equations (see equation (1) above) solve for the species densities as a function of time, but the time-dependence can be translated into a spatial dependence, i.e., as a function of position in the arc column, based on the gas velocity, due to the similarity between a batch reactor and a plug flow reactor. The same method was also applied in our previous work [5,11,12,15,30,32–34,48].

However, some assumptions need to be made:

- Trenchev et al. [38] and Ramakers et al. [23] have revealed that the plasma density and the arc width do not change significantly with electrical current and gas flow rate, and thus we adopt a constant arc radius for all calculations. Based on 3D turbulent gas flow pattern calculations using the SST (Shear Stress Transport) RANS (Reynolds-

Averaged Navier- Stokes) turbulent model [49], in combination with a 3D fluid plasma model, explained in [38], the actual arc in the GAP seems to have a radius of 1 mm. However, the temperature just outside the arc is still high enough to induce plasma, and therefore CO_2 dissociation. Moreover, the 3D calculations were performed in argon, and CO_2 will be characterized by higher gas temperatures, due to the presence of VT-relaxation, so the arc region in a CO_2 plasma will be wider. Finally, due to the skewed spiral motion of the arc, the actual volume covered by the arc will be somewhat larger than predicted by the 3D-2D fluid simulations. Therefore, we assume a constant arc radius of 2 mm, which – in combination with a total arc length of 39.6 mm (see Figure 1), results in a total plasma volume of 497.6 mm^3. Still, not all gas flowing in the reverse vortex, which has more or less the same radius as the outlet (i.e., 3.54 mm) [24], will be treated by the arc plasma. Therefore, further research will be needed to improve the gas inlet configuration and the reactor design, in order to enhance the amount of gas treated by the plasma.

- The initial gas temperature, i.e. right before entering the arc region, is set to room temperature (293.15 K). Inside the arc, the gas will quickly heat up. The actual gas temperature inside the arc is adopted from 3D fluid model calculations [24], and not self-consistently calculated in the present model. Indeed, the latter might be too approximative, as it only accounts for gas heating due to collisions and chemical reactions, and heat loss to the environment, but not taking turbulent heat losses into account, which are stated to be important in the GAP [24]. However, the position in the arc at which this gas temperature is reached, is determined by solving equation (3). As soon as this gas temperature is reached, the value is kept constant for the rest of the arc column (see below), based on [24].

- A constant mass flow rate through the reactor is assumed and the pressure is held constant at atmospheric pressure, in agreement with the 3D fluid dynamics calculations of Trenchev et al. [24]. Since the gas temperature will rise as a function of residence time (or position in the arc), the particle densities will decrease, in order to maintain constant pressure. Furthermore, the gas velocity will increase to conserve the mass flow rate. As the conservation equations for the various species (equations (1)) do not account for gas expansion at constant pressure, we calculate the gas pressure at every time step of the simulation from the actual species densities and gas temperature, and the species densities are then corrected to maintain a constant (atmospheric) pressure, following the approach of Kozak et al. [12].
- The initial gas velocities in the arc region, at each gas flow rate considered in this study, are adopted from the 3D gas flow patterns calculated by the fluid dynamics model of [24]. The corresponding velocities are 1.96, 2.55, 3.14, 3.72 and 4.31 m/s, for gas flow rates of 10, 13, 16, 19, and 22 L/min, respectively. These velocities are updated during each time step of the simulation, as described above, to maintain constant mass flow rate and pressure.

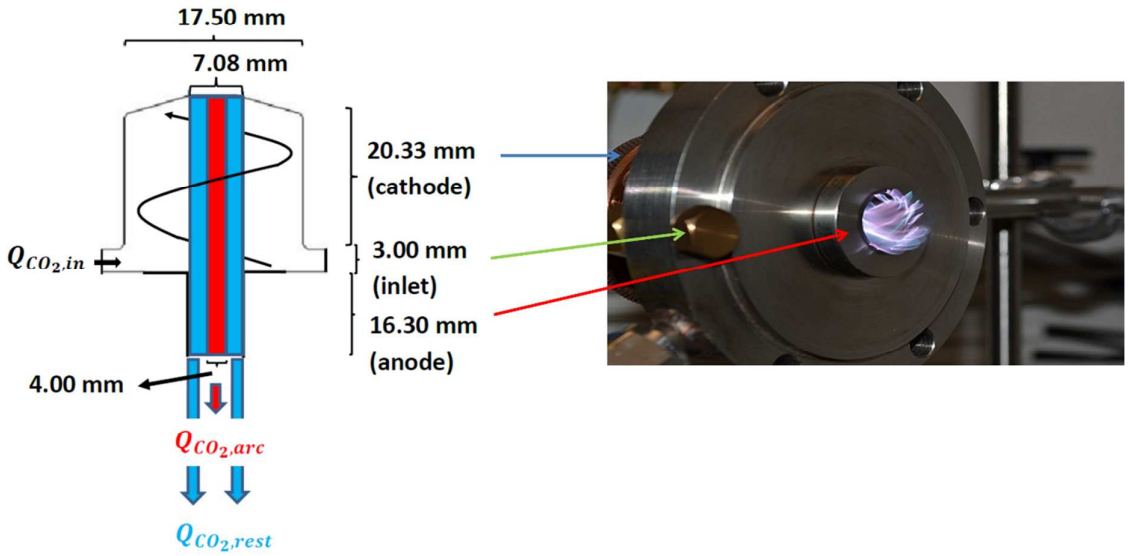

Figure 1: Schematic diagram of the GAP, with characteristic dimensions of cathode (reactor body), inlet region (insulator), anode (outlet) and arc region, and indication of the outer vortex (solid spiral). The inner (reverse) vortex is not depicted for the sake of clarity, but it is confined in the red and blue rectangles. The red rectangle shows the arc region, as considered in the model. $\boldsymbol{Q_{CO_2,in}}$, $\boldsymbol{Q_{CO_2,arc}}$ and $\boldsymbol{Q_{CO_2,rest}}$ denote the flux of CO_2 entering the reactor, and leaving the arc and the rest of the reactor, respectively (see text for more explanation).

The CO_2 conversion after passing through the arc, $X_{CO_2,arc}$, is defined as:

$$X_{CO_2,arc}(\%) = 100\% \left(1 - \frac{n_{CO_2,e}\, v_e}{n_{CO_2,i}\, v_i}\right) \quad (4)$$

where $n_{CO_2,e}$ and v_e are the CO_2 density (in m^{-3}) and gas velocity (in m s^{-1}) at the end of the arc region near the outlet, and $n_{CO_2,i}$ and v_i are the CO_2 density (in m^{-3}) and gas velocity (in m s^{-1}) at the beginning, right before entering the arc region, i.e., at room temperature. Note that the same formula can be used to calculate the CO_2 conversion as a function of position in the arc, simply by using the CO_2 density and gas velocity at that position in the arc.

Since not all gas in the reactor passes through the arc region, the total CO_2 conversion in the reactor, which is also measured experimentally, will be lower than the CO_2 conversion after passing through the arc region, as we also need to account for the unconverted CO_2 in the reactor. This total conversion, $X_{CO_2,tot}$, is defined as:

$$X_{CO_2,tot}(\%) = 100\%(1 - \frac{Q_{CO_2,arc}+Q_{CO_2,,rest}}{Q_{CO_2,in}}) \quad (5)$$

where $Q_{CO_2,in}$, $Q_{CO_2,arc}$ and $Q_{CO_2,,rest}$ are the CO_2 fluxes (in s^{-1}) entering the reactor, exiting the arc region at the outlet and exiting the reactor without passing through the arc, hence without being converted. This means that we need to define the fraction of CO_2 that passes through the arc region, which is explained below.

The CO_2 flux entering the reactor $Q_{CO_2,in}$ is defined as:

$$Q_{CO_2,in} = n_{CO_2,i}\,\dot{V} \quad (6)$$

where $n_{CO_2,i}$ is the CO_2 density (in m^{-3}) at the inlet of the reactor (at room temperature) and $\dot{V}$ the volumetric flow rate (in $m^3\ s^{-1}$). The CO_2 flux exiting the arc region at the outlet $Q_{CO_2,arc}$ is defined as:

$$Q_{CO_2,arc} = n_{CO_2,e}\,v_e\,A_{arc} \quad (7)$$

with $n_{CO_2,e}$ and v_e the CO_2 density (in m^{-3}) and gas velocity (in $m\ s^{-1}$) at the end of the arc region near the outlet, and A_{arc} the cross sectional area of the arc region, i.e. 12.57 mm^2 .

Finally, due to conservation of mass, the CO_2 flux $Q_{CO_2,,rest}$ which is not treated by the plasma, is given by:

$$Q_{CO_2,rest} = Q_{CO_2,in} - n_{CO_2,i}\, v_i\, A_{arc} \quad (8)$$

Hence, the fraction of CO_2 that passes through the arc region is defined by the mass flow rate through the arc, and is 14.8 % of the total mass flow rate through the reactor. The remaining 85.2% does not pass through the arc, and will not be converted.

The energy efficiency (E_{eff}) is defined as:

$$E_{eff}(\%) = \frac{X_{CO_2,tot}(\%) * \Delta H}{SEI} \quad (9)$$

with ΔH the energy cost of splitting one CO_2 molecule into CO and ½ O_2, i.e. 2.9 eV/molec, and SEI the specific energy input (in eV/molec), which is calculated as:

$$SEI = \frac{P_{plasma} * k_b * T_{gas,in}}{p * \dot{V} * 1.60 * 10^{-19}} \quad (10)$$

with P_{plasma} the plasma power (in W), k_b the Boltzmann constant (in J K^{-1}), $T_{gas,in}$ the gas temperature at the reactor inlet (i.e. 293.15 K), p the pressure (i.e. 1.01325x10^5 Pa) and $\dot{V}$ the volumetric flow rate (in m^3 s^{-1}). $1.60x10^{-19}$ (J/eV) is a conversion factor to change the units of J into eV.

The vibrational temperature T_v is calculated from the densities of the various asymmetric mode levels, assuming that they follow a Boltzmann distribution:

$$T_v(K) = \frac{1}{i}\sum_{i=1}^{k} \frac{(-E_{i-1}+E_i)*11605}{\ln(\frac{n_i}{n_{i-1}})} \quad (11)$$

with E_i and E_{i-1} the energies (in eV) of the ith and (i-1)th asymmetric mode level and n_i and n_{i-1} the densities (in m^{-3}) of the ith and (i-1)th asymmetric mode level. 11605 is a conversion factor to change the units of eV into K and k is the number of asymmetric mode levels taken into account, which follow a (quasi) Boltzmann distribution. In the beginning of the arc column (i.e., first 0.30 cm), only the first asymmetric mode level is taken into account (k =1) in calculating the vibrational temperature, since the vibrational distribution function (VDF) does not exhibit a Boltzmann distribution for higher levels for all flow rates studied (see Figure S.1 in the Supporting Information). Between 0.30 and 0.60 cm, the first four asymmetric mode levels are taken into account (k =4), between 0.60 and 0.90 cm the first seven (k =7), and after 0.90 cm the first ten asymmetric mode levels (k =10) are taken into account, as they follow a Boltzmann distribution here (see Figure S.1 in the Supporting Information). The energies of the different vibrational levels included in the model are listed in the Supporting Information (Table S.1).

3. Results and discussion

3.1. Plasma characteristics inside the arc

To understand the CO_2 conversion in the GAP, we first need to obtain a good insight in the main plasma characteristics defining the CO_2 conversion, i.e., the gas temperature, vibrational temperature, electron temperature and electron number density. They are plotted as a function of position in the arc column in Figure 2 for different flow rates, ranging from 10 till 22 L/min, i.e., the same values as used in the experiments of [23]. We use a plasma power of 650W, lying somewhat in the middle of the experimental range (529 – 712 W), used in [23].

As is clear from Figure 2(a), the gas temperature rises quickly till its maximum defined value of 3340 K. Although this gas temperature seems quite high, 3D-2D fluid simulations show that the arc temperature in CO_2 is around 3100 K for a plasma power of 500 W [24]. In this work, we consider a power of 650 W, so we assume a slightly higher gas temperature in the arc. Furthermore, the rotational/gas temperature in a similar setup was measured in [22], obtaining values of 2700±50 K for a CO_2 plasma, doped with 1% N_2 for a plasma power of 200 W. Since our plasma power is more than three times higher, we believe the assumption of the arc temperature being 3340 K is reasonable. Nevertheless, it has to be realized that it is only an estimation. As the temperature inside the arc is very high, thermal decomposition of CO_2 is included in our model through the reactions $CO_2 + M \rightarrow CO + O + M$ and $CO_2 + O \rightarrow CO + O_2$, including their reverse processes. Our calculations reveal that thermal conversion is responsible for about 90 % of the total CO_2 conversion at this high temperature. This maximum is reached faster at lower flow rates (i.e., even at 0.5 cm for 10 L/min), which is logical, as the gas has more time to heat up. The vibrational temperature (Figure 2(b)) and electron density (Figure 2(d)) follow the same trend, achieving their maximum values (~ 3340 K and 8.5×10^{11} cm^{-3}, respectively) at the same positions. We were not able to compare the electron density with experimental values, and we are not aware of such measurements in a CO_2 GAP. In a conventional GA the electron density in air was measured to be 10^{12}-10^{13} cm^{-3} [50]. However, CO_2 has more internal degrees of freedom than N_2 and O_2, so we expect less electron energy going to ionization and more towards vibrational excitation, which can explain the lower electron density than in air. The fact that our calculated values are rather low may be attributed to the 0D approach, which does not capture non-uniformity in the arc discharge, e.g., higher power density in the center, which may lead to higher electron densities. However, according to [22], the GAP operates in the transitional regime where the

electron density lies typically in between 10^{11} and 10^{12} cm^{-3}, so we think our values are reasonable."

The initial electron temperature (Figure 2(c)) is equal to 2.3 eV and it lowers to 1.1 eV when the maximum gas temperature is reached. This higher electron temperature in the beginning of the arc can be attributed to the fact that the power is initially deposited over a small number of electrons. The values obtained for the gas and electron temperature are typical for the GAP and other types of so-called warm plasma [22,24,38].

The electron temperature is much higher than the gas temperature (1.1 eV or 12800 K versus 3340 K) and thus the plasma is in non-equilibrium, which is most suitable to activate the gas through electron impact dissociation, ionization and excitation, and thus for energy-efficient CO_2 conversion.

Initially, the vibrational temperature is about two times higher than the gas temperature, indicating that the vibrational levels are overpopulated, and show a non-thermal vibrational distribution function (VDF) (see Figure S.1 in the Supporting Information). The vibrational temperature also exhibits a sharp increase, showing the importance of vibrational excitation in a GAP, as also stated in [21]. However, the sharp increase in vibrational temperature happens at the same positions as the gas temperature, and both temperatures become almost equal to each other, which means that the vibrational levels will become thermalized after a travelled distance larger than 0.60 cm, and they will exhibit a near Boltzmann distribution (see Figure S.1 in the Supporting Information). Therefore, the highest vibrational levels will not be overpopulated, which would be needed for the most energy efficient vibration induced dissociation from the highest levels (see further).

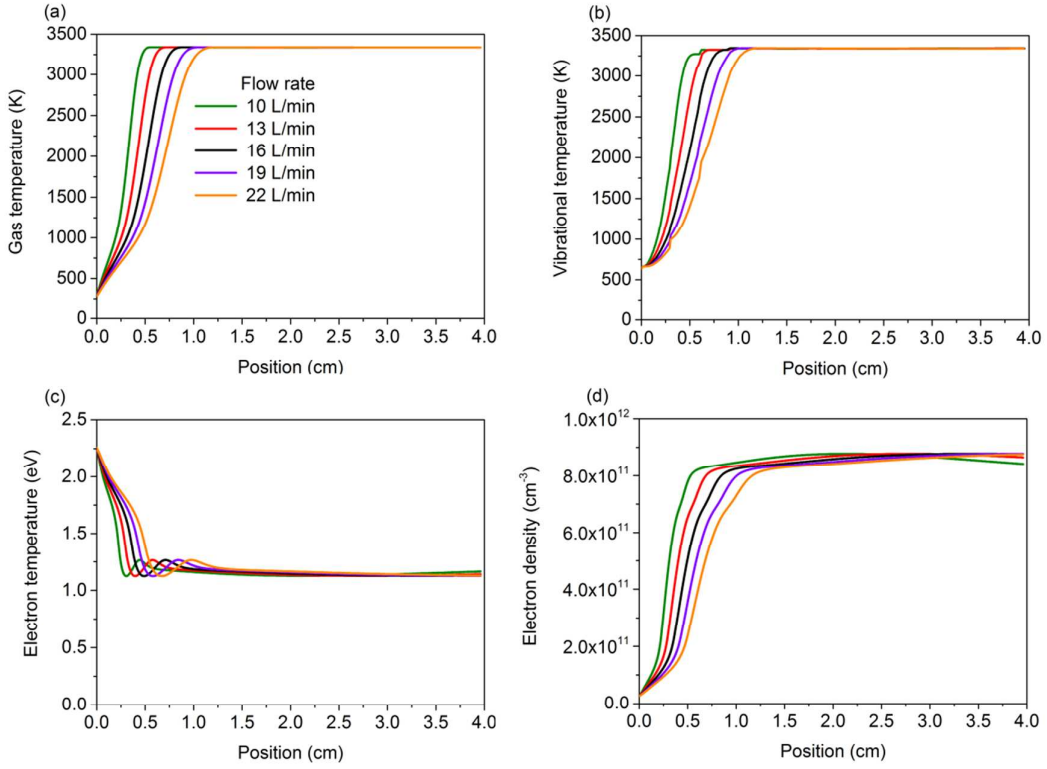

Figure 2: Gas temperature (a), vibrational temperature (b), electron temperature (c) and electron density (d) as a function of position in the arc column, calculated for different gas flow rates, at a plasma power of 650 W.

Figure 3 shows the evolution of the CO_2 conversion inside the arc, as a function of position in the arc column, for different flow rates and a plasma power of 650 W. The conversion starts to increase when the vibrational and gas temperature reach their maximum values. This indicates that vibration induced dissociation will play a significant role (see also sections 3.3 and 3.4).

The conversion is higher at lower flow rates, which is again logical, because the gas has more time to be converted. At 22 L/min, the conversion rises more or less linearly, up to 35% at the end of the arc column. At 10 L/min, the conversion reaches more than 50% at the end of the arc column, but after a linear increase up to 1.5 cm, the rise becomes less

significant, indicating that the reverse reaction (i.e., recombination of CO into CO_2) will become important as soon as about 30% of the CO_2 molecules are converted (see also section 3.3 below).

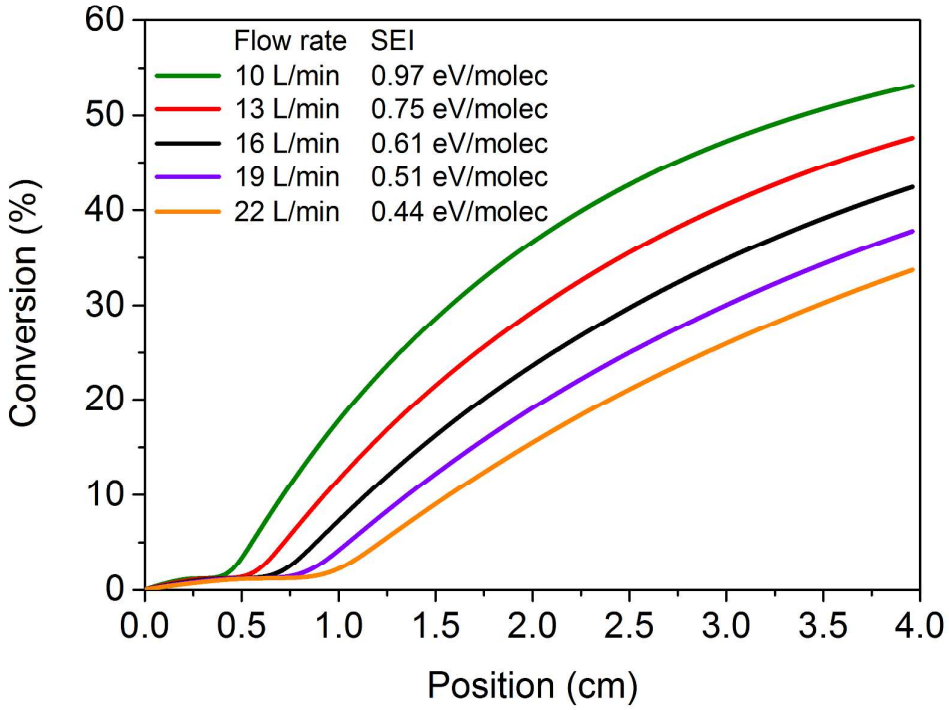

Figure 3: Calculated CO_2 conversion inside the arc, as a function of position in the arc column, for different gas flow rates, at a plasma power of 650 W. The corresponding values of specific energy input (SEI), calculated from the plasma power and gas flow rate (see equation (10)), are also indicated.

3.2 Overall CO_2 conversion and energy efficiency

The overall CO_2 conversion will be lower than the values obtained inside the arc, as a significant fraction of the gas (i.e., about 85%) does not pass through the arc column and will not be converted. Thus, we have to multiply the CO_2 conversion at the end of the arc column

with 14.8%, to obtain the overall CO_2 conversion, as explained in detail in section 2.3 above. The latter is illustrated in Figure 4 as a function of SEI, together with the experimentally obtained conversions, as well as the energy efficiencies (calculated with equations (5), (9) and (10) in section 2.3), for the conditions studied in [23], i.e., different combinations of gas flow rate and plasma power. It is clear that the overall conversion is more limited, i.e., maximum around 8%. The calculated conversions and energy efficiencies show good agreement with the experimental results, with an average relative error of 6% and a maximum relative error of 16 % at SEI = 0.48 eV/molec.

Both the model and the simulations indicate energy efficiencies up to 33 % for a CO_2 conversion of 7.5%. Similar values of conversion between 2 % and 9 % and energy efficiencies between 22 % and 37 % were achieved in the GAP of [21]. Furthermore, in an AC-pulsed reverse vortex "tornado" flow GA plasma [25], a CO_2 conversion of 6 % with a corresponding energy efficiency of 29 % was obtained, again very similar to our results. These energy efficiencies are somewhat higher than earlier experiments with conventional GA plasmas, where maximum energy efficiencies of approximately 25 % were reported [18], but at higher conversions of 18 %. In a recent study of a conventional GA [20], conversions in the range of 6-10 % were found with energy efficiencies between 20% and 40%, which is comparable and even slightly better than our results. However, in this case, the GA was sealed in an insulated container, providing for recirculation of the gas through the arc, and hence a larger fraction of the gas can be treated.

Snoeckx and Bogaerts recently reported a very detailed comparison of the CO_2 conversion and energy efficiency in all types of plasmas that have been investigated up to now [4], which showed that the GAP is among the most energy efficient plasma sources for CO_2 conversion. The highest energy efficiencies ever measured were in a microwave (MW) discharge with values up till 60 % [14,51] and even 80-90 % [13,16]. However, the latter results

were obtained using supersonic flows combined with reduced pressure, and the latter is undesirable for upscaling to an industrial scale. Furthermore, when MW plasmas operate at atmospheric pressure, the energy efficiency typically drops to 5-20 % [17]. One of the most suitable reactors for upscaling is the DBD reactor, due to its robust design and its operation at atmospheric pressure. However, the energy efficiency is generally (much) lower than in a GA, with values typically reported up to maximum 10-15%, although recently energy efficiencies up till 23 % were achieved for a CO_2 conversion of 26 % in a DBD in burst mode [6].

Although the GAP thus shows promising results, also in comparison with other plasma types, the conversion and energy efficiency should still be improved for further exploitation. As there is very good agreement between the calculated and experimental conversions and energy efficiencies, we may conclude that the model provides a realistic picture of the CO_2 conversion, and that it can thus be used to elucidate the underlying reaction pathways, which is needed to further improve the performance. This will be discussed in the next section.

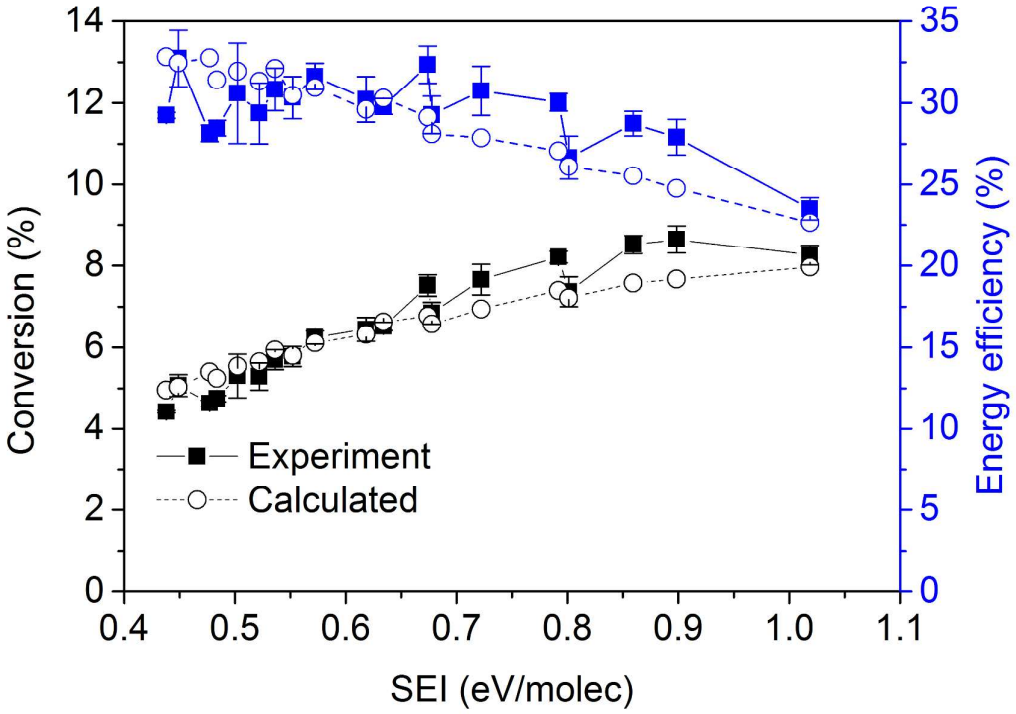

Figure 4: Calculated and measured CO_2 conversion (left y-axis) and corresponding energy efficiency (right y-axis) as a function of the specific energy input (SEI), which is a combination of different values of gas flow rate and plasma power. The experimental data are adopted from [23].

3.3 Chemical pathway analysis of CO_2 conversion

In Figure 5 we plot the rates, integrated over the entire residence time of the gas inside the plasma, of the most important loss and formation processes of CO_2, as a function of SEI. The total time-integrated rate of the loss processes is only about a factor 2-3 higher than the total time-integrated rate of the formation processes, i.e. 1.0-2.5x10^{18} cm^{-3} versus 2.3x10^{17}-1.3x10^{18} cm^{-3}, for all conditions investigated. This indicates that a significant fraction of the dissociated CO_2 (in CO, O and O_2) will recombine again inside the plasma. Indeed, the reaction products of the dissociation processes are also the most important reactants for the formation of CO_2, as will be explained below.

It is clear from Figure 5(a)) that vibration induced dissociation plays a significant role in converting CO_2. The most important dissociation processes are the collisions of vibrationally excited CO_2 with an O atom, forming CO and O_2, followed by the collision with any neutral species (denoted as M), forming CO and O. Electron impact dissociation from the ground state and from the vibrationally excited states of CO_2 also play a role, but their rates are about three times lower.

The most important formation mechanism of CO_2 (see Figure 5b) is the reaction between CO and O_2, forming again CO_2 and an O atom, followed by the three body recombination ($CO + O + M \Rightarrow CO_2 + M$), although the rate of the latter process is almost one order of magnitude lower.

Since the most important formation processes are the reverse of the most important loss processes, we need to look at the net rates of these processes (i.e., loss minus formation), depicted in Figure 5(c). It is clear that dissociation upon collision with an O atom or any neutral species M, primarily from vibrationally excited CO_2, contribute almost equally towards the CO_2 dissociation, with relative contributions of 38% and 40% at the lowest and highest SEI value, respectively. These processes are followed by electron impact dissociation from the ground state (14% and 10% at the lowest and highest SEI value) and from vibrationally excited CO_2 (~7%, independent of the SEI).

A general reaction scheme illustrating the main pathways of CO_2 dissociation in the GAP is given in Figure 6. The process is initiated by electron impact excitation from the CO_2 ground state, populating the vibrational levels (black arrows). Furthermore, the lowest vibrational levels ($CO_2(v_i)$) collide with each other, gradually populating the higher vibrational levels ($CO_2(v_{j>i})$) by so-called VV relaxation (yellow arrows). At the same time, the vibrational levels also collide with neutral species in so-called VT relaxation (red arrows), which leads to loss of the higher levels, and thermalization of the VDF. The VV relaxation is

thus generally beneficial for energy-efficient CO_2 conversion, while the VT relaxation has a negative effect. The dissociation of CO_2 occurs upon collision with O atoms (blue arrows), any neutral species M (green arrows) and electrons (black arrows), mainly from the CO_2 vibrational levels, although electron impact dissociation mainly happens from the ground state (see Figure 5). At the same time, recombination of CO with O or O_2 also takes place, forming again CO_2 (purple arrows), which should be avoided.

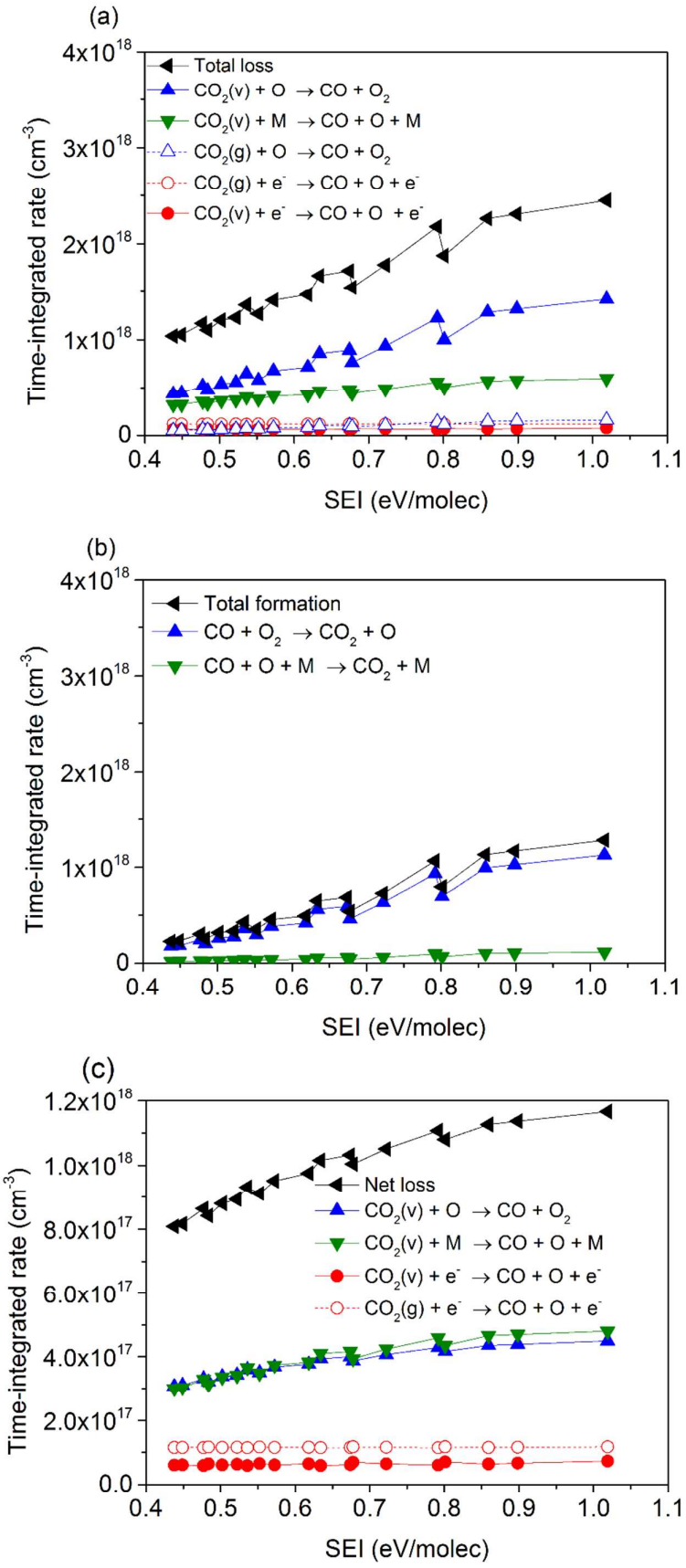
(a)
Total loss
CO2(v) + O → CO + O2
CO2(v) + M → CO + O + M
CO2(g) + O → CO + O2
CO2(g) + e- → CO + O + e-
CO2(v) + e- → CO + O + e-
Time-integrated rate (cm-3)
SEI (eV/molec)
(b)
Total formation
CO + O2 → CO2 + O
CO + O + M → CO2 + M
Time-integrated rate (cm-3)
SEI (eV/molec)
(c)
Net loss
CO2(v) + O → CO + O2
CO2(v) + M → CO + O + M
CO2(v) + e- → CO + O + e-
CO2(g) + e- → CO + O + e-
Time-integrated rate (cm-3)
SEI (eV/molec)

Figure 5: Time-integrated rates of the main loss (a) and formation (b) mechanisms of CO_2, and of the main net loss mechanisms (c), as a function of the specific energy input (SEI). The same colors are used in (a,b,c) for the same processes; solid lines/closed symbols are used for the processes from the vibrational levels, while dashed lines/open symbols apply to the processes from the ground state.

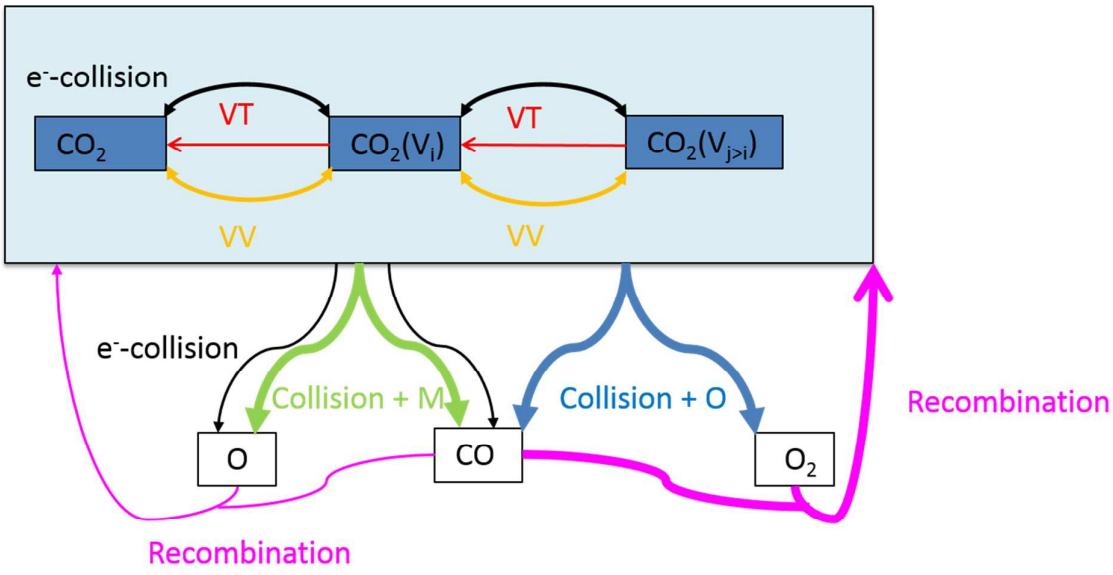

Figure 6: Reaction scheme illustrating the main pathways for CO_2 conversion in the GAP.

3.4 Role of the vibrational levels in the CO_2 dissociation

It is clear from Figure 5 that most of the CO_2 dissociation occurs from the vibrational levels. To understand which vibrational levels contribute most, we plot in Figure 7 the net contribution of the different vibrational levels towards the dissociation of CO_2 at 650 W, for different flow rates, as well as the main dissociation processes occurring at each vibrational level, at a flow rate of 16 L/min. As shown in Figure 7(a), for all flow rates studied, most dissociation occurs from the symmetric mode vibrational levels (i.e., combined levels Va-Vd; see Table S.1 in the Supporting Information for the identification of these levels; overall contribution ~ 65 %), followed by the ground state (contribution ~16 %) and the first three

asymmetric mode vibrational levels (overall contribution~ 10 %). The remaining 9 % of the CO_2 dissociation arises from the higher asymmetric mode levels. This low contribution is due to the fact that the vibrational distribution function (VDF) quickly becomes quasi-Boltzmann distributed, at positions > 0.60 cm (see Figure S.1 in the Supporting Information). This means that the highest levels will not be overpopulated, as is the case for instance in MW plasmas at reduced pressure [11,15,34]. Therefore, dissociation will occur from the lowest levels instead of from the more desirable highest levels. Indeed, at atmospheric pressure and high gas temperatures, VT relaxation will play an important role in thermalizing the VDF. The same was observed in [15,16] for a MW discharge at atmospheric pressure.

Figure 7(b) demonstrates that vibration induced dissociation of the symmetric mode levels, upon collision with an O atom or a neutral species M, contribute most to the dissociation of CO_2, while electron impact dissociation mainly occurs from the CO_2 ground state. This process, as well as collision with an O atom, becomes less important upon increasing asymmetric mode level. Indeed, for these higher levels, dissociation upon collision with any neutral species M is the most important. Since most dissociation occurs from the lowest levels, we will not further discuss the dissociation kinetics from the higher asymmetric mode levels.

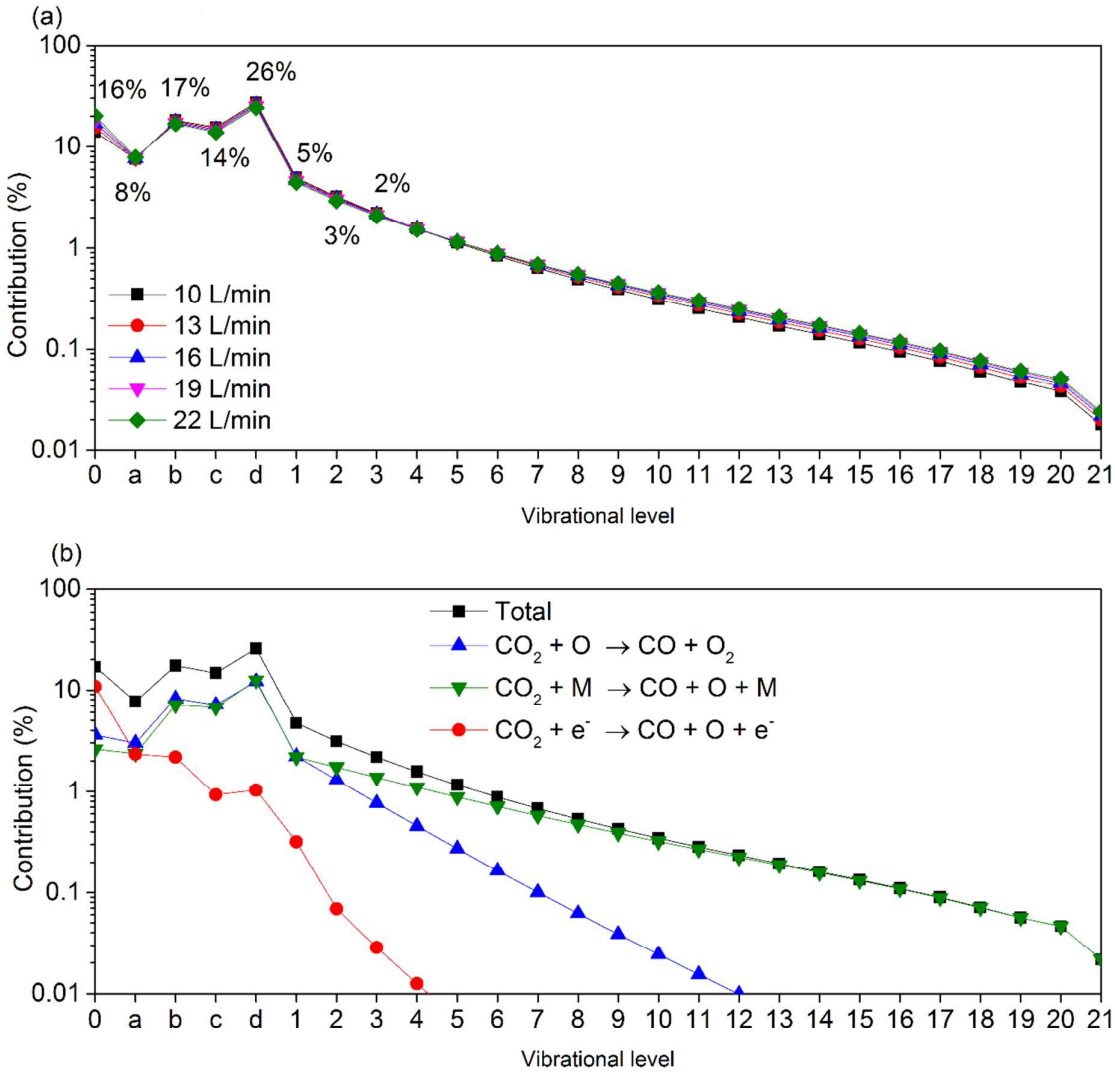

Figure 7: Relative contribution of the different vibrational levels of CO_2 to the total dissociation of CO_2 for different flow rates at an input power of 650 W (a), and contributions of the individual processes for each vibrational level, at a flow rate of 16 L/min and an input power of 650 W.

3.5 Optimizing the CO_2 conversion and energy efficiency

Although the GAP already performs quite well compared to other plasma types [4], it is clear that there is still room for improvement, if we could exploit better the role of the higher vibrational levels or if we could reduce the rate of the CO_2 formation. 0D kinetic modelling

allows us to study the effect of different plasma conditions, beyond what is experimentally feasible until now, on the CO_2 chemistry, and thus on the CO_2 conversion and energy efficiency, to give conceptual information about how to improve the GAP. In the following subsections, we study the effect of (i) lowering and increasing the gas temperature, as this will affect the VDF [15], and (ii) removing the O_2 molecules, in order to block the main formation process of CO_2. We also extend the range of SEI values from 0.1 eV/molec to 2.5 eV/molec, so we investigate a wide range of powers (between 147 W and 33.4 kW) and gas flow rates (between 22 L/min and 200 L/min). It should be realized that some combinations, such as high SEI values and low gas temperatures, cannot yet be experimentally achieved, but the results might give valuable insights for future reactor design. The flow rates used in the following subsections are 22 and 200 L/min. Indeed, the highest energy efficiency in our experiments was obtained for 22 L/min [23], and on the other hand, flow rates around 200 L/min were applied in [52] where a high power GAP was designed for upscaling towards industrial applications.

The predicted conversions and energy efficiencies as a function of flow rate between 22 and 200 L/min, and for different values of the SEI, are plotted in Figures S.2 and S.3 in the Supporting Information, at a maximum gas temperature of 500 K and 3500 K, respectively. A gradual change is observed in both conversion and energy efficiency, between the values obtained at 22 L/min and 200 L/min. Therefore, in the following, we only show results for this minimum and maximum flow rate.

3.5.1 Influence of the gas temperature

As mentioned above, a high gas temperature enhances the VT relaxation, which has a negative effect on energy-efficient CO_2 conversion as it depopulates the higher vibrational

levels. On the other hand, the rates of the dissociation reactions upon collision with O atoms or any neutral species M will also rise with temperature. Therefore, we want to investigate the effect of the maximum gas temperature in the arc column on the CO_2 conversion and energy efficiency. The results are shown as a function of SEI in Figure 8 for a flow rate of 22 L/min and 200 L/min. In both cases, we vary the SEI between 0.1 and 2.5 eV/molec. This corresponds to a plasma power between 147 W and 3.68 kW for a flow rate of 22 L/min, while at 200 L/min, this corresponds to values between 1.34 kW and 33.4 kW.

At 22 L/min (Figure 8(a,b)), the power seems too low for sufficient electron impact vibrational excitation followed by vibrational pumping towards the highest levels, and thus for dissociation from these highest levels, at all SEI values studied. At a low gas temperature of 500 K, where VT relaxation is suppressed, our calculations predict that dissociation upon collision with neutral species does not contribute at all towards CO_2 dissociation, and dissociation is almost entirely by electron impact dissociation from the ground state and the lowest vibrational levels. This is true for the entire range of SEI values (see Figures S.4(a) and S.5(a) in the Supporting Information for an SEI of 2.5 eV/mole and 0.2 eV/molec, respectively). Especially at low SEI values, electron impact dissociation mainly occurs from the ground state (see Figure S.5(a)). This process is less energy efficient than dissociation from the vibrational levels upon collision with neutral species. Thus, the CO_2 conversion and energy efficiency will rise with increasing gas temperature for 22 L/min, as is obvious from Figure 8(a,b), because dissociation upon collision with neutral species (either O atoms or any molecule M) from the (low) vibrational levels becomes more and more important at higher gas temperature (cf. Figure S.4(b) and S.5(b) in the Supporting Information, where these processes are shown to be dominant for a gas temperature of 3500 K and an SEI of 2.5 eV/molec and 0.2 eV/molec, respectively).

As illustrated in Figure 8(a,b), at this flow rate of 22 L/min, a maximum conversion of 9 % is obtained at 3500 K and an SEI of 2.5 eV/molec, but it corresponds to a low energy efficiency of 10 %, while a maximum energy efficiency above 80 % is predicted at the same temperature but at an SEI of 0.2 eV/molec, corresponding to a low conversion of 6 %. It should, however, be noted that in reality, temperatures of 3500 K are highly unlikely at an SEI below 0.34 eV/molec, and thus, an external heat source would be necessary to achieve this temperature. This would yield a higher overall SEI and thus lower energy efficiencies.

At a flow rate of 200 L/min (Figure 8(c,d)), the CO_2 conversion and energy efficiency follow the same trend as for 22 L/min, for SEI values below 0.7 eV/molec, with rising conversion and energy efficiency at higher temperatures. The maximum energy efficiency in this range was calculated to be 15 %, at an SEI of 0.34 eV/molec and 3500 K. In this case, dissociation upon collision with O atoms or molecules M also plays a significant role, although it is less significant than at 22 L/min, due to the higher plasma power for the same SEI and thus a larger contribution of electron impact dissociation (see Figure S.6 in the Supporting Information). As the latter process is less energy efficient than dissociation upon collision with neutral species, this explains the lower energy efficiency.

For SEI values above 0.7 eV/molec, the behavior at 200 L/min is different from that at 22 L/min. Indeed, the conversion and energy efficiency rise upon lowering the gas temperatures to 1000 K and especially 500 K (see Figure 8(c,d)). The reason is that vibrational excitation followed by vibrational pumping, and hence vibration induced dissociation from the highest levels, now becomes dominant, as can be deduced from Figure S.7(a) in the Supporting Information. Indeed, the contribution of vibration induced dissociation from the highest vibrational levels is now 81 %, which is the most desired way of dissociating CO_2. However, this situation is only reached at very high plasma powers, to obtain these high SEI values (above 0.7 – 1 eV/molec) at the flow rate of 200 L/min, and thus

the energy efficiency (maximum 25 %) is still lower than the values we obtained in our experiments [23], but the corresponding conversion is somewhat higher (ca. 12%) than our best values [23]. At higher gas temperatures, the CO_2 conversion and energy efficiency drop due to thermalization of the VDF, until 3000 K where it rises again due to the increasing importance of dissociation upon collision with the neutral species (see also Figures S.7(b) and S.7(c) in the Supporting Information).

We may thus conclude that for low flow rates (e.g., 22 L/min), a higher gas temperature leads to a higher conversion and energy efficiency, which is attributed to thermal dissociation. This is true at all SEI values (and thus powers) investigated, but the energy efficiency is maximum at low SEI. On the other hand, at high flow rates and sufficiently high SEI values (and thus very high power values), electron impact vibrational excitation followed by pumping, and thus vibration induced dissociation from the highest levels, becomes much more significant at lower gas temperatures, due to less VT relaxation, and therefore, at these conditions, lower gas temperatures lead to higher conversion and energy efficiency.

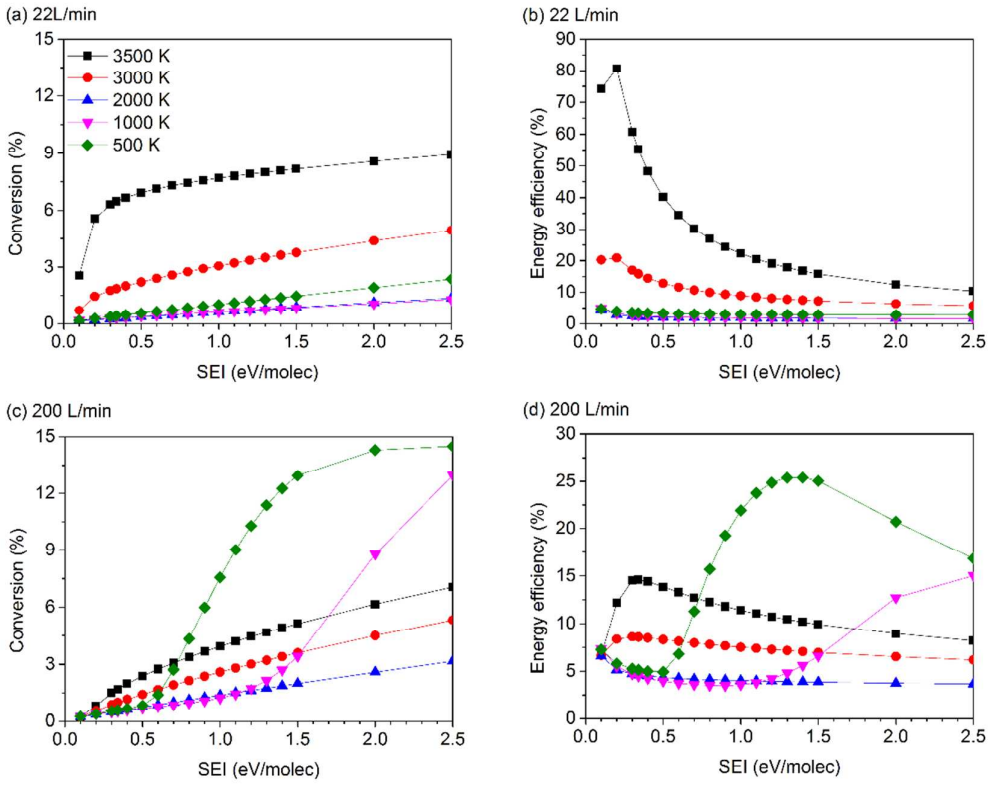

Figure 8: CO_2 conversion (a, c) and energy efficiency (b, d) as a function of SEI for different maximum gas temperatures in the arc column, at a flow rate of 22 L/min (a, b) and 200 L/min (c, d). The plasma power values needed to reach this SEI range vary between 147 W and 3.68 kW for 22 L/min, and between 1.34 kW and 33.4 kW for 200 L/min.

3.5.2 Removing the O_2 molecules

As shown in Figure 5, the total rate of CO_2 formation is only 2-3 times lower than the total rate of CO_2 loss, and this is mainly attributed to the recombination of CO with O_2 molecules. Hence, we want to find out with the model whether removing the O_2 molecules from the system can improve the overall CO_2 conversion. Methods to realize this could be centrifugation, distillation and absorption, but they are difficult and not energy efficient, due to the small difference in molar mass of CO and O_2.[53,54] Nevertheless, we investigate here this effect theoretically, because novel and more energy efficient methods might be

developed in future. The effect of removing the O_2 molecules from the system on the CO_2 conversion and energy efficiency is presented in Figure 9, for a flow rate of 22 L/min and 200 L/min, and typical maximum arc temperatures of 3000 and 3500 K.

At a flow rate of 22 L/min, O_2 removal has a slightly positive effect on the CO_2 conversion and energy efficiency at both temperatures investigated (see Figure 9(a,b)). The reason why the effect is so small is the following. When O_2 is removed, the CO_2 formation process due to recombination of CO with O_2 ($CO + O_2 => CO_2 + O$) is indeed zero, but it also means that no O atoms can be formed by this process. Furthermore, no O atoms can be formed by dissociation of O_2 either. Hence, the O atom density drops significantly, and dissociation upon collision of vibrationally excited CO_2 with O atoms will also drop. Thus, not only the CO_2 formation decreases, but the CO_2 loss drops as well. Therefore, the net positive effect of O_2 removal on the CO_2 conversion and energy efficiency is very small**.** At 200 L/min, the effect of O_2 removal is even completely negligible (see Figure 9(c,d)).

In order to realize a higher CO_2 conversion, it would thus be necessary to remove the O_2 molecules, but at the same time the O atom production should not be disturbed or (more realistically) it should be replaced by another active agent that can contribute to CO_2 dissociation, such as H atoms. Adding a hydrogen source like CH_4 or H_2 might thus provide a solution. Indeed, the combined CO_2/CH_4 conversion (or dry reforming of methane) [25] and CO_2/H_2 conversion [21] typically yield a higher CO_2 conversion and energy efficiency.

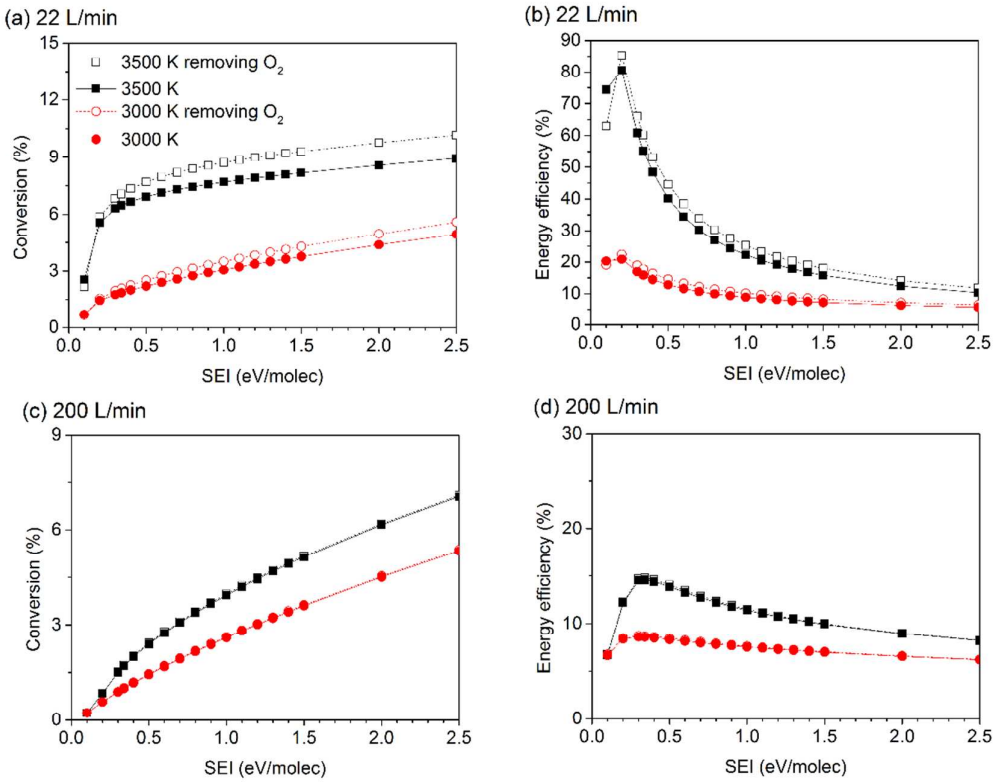

Figure 9: CO_2 conversion (a, c) and energy efficiency (b, d) as a function of SEI for 22 L/min (a, b) and 200 L/min (c, d), when the O_2 molecules are artificially removed from the system (dashed lines, open symbols) or not (solid lines, filled symbols).

4. Conclusion

We presented a chemical kinetics study to elucidate the main dissociation mechanisms of CO_2 in a GAP, with special emphasis on the role of the vibrational kinetics. The CO_2 conversion and energy efficiency calculated with the model in a wide range of SEI values (corresponding to different values of power and gas flow rate) are in good agreement with experimental values, obtained at the same conditions. This indicates that the model can provide a realistic picture of CO_2 conversion in the GAP, and can thus be used to identify the limitations, and propose solutions for further improvement.

The results obtained, both experimentally and in the model, demonstrate that the GAP is promising for CO_2 conversion, with energy efficiencies ranging between 23 and 33 %. This is explained by the large contribution of dissociation of the vibrationally excited levels upon collision with an O atom (CO_2 + O => CO + O_2) or any neutral species M (CO_2 + M => CO + O + M). However, because of the high gas temperature in the GAP, the VDF exhibits a quasi-Boltzmann distribution with low population of the highest vibrational levels. Therefore, the dissociation mainly occurs from the lowest symmetric mode levels (contribution ~ 65 %), followed by the ground state (contribution ~ 16 %) and the first three asymmetric mode levels (contribution ~ 10%), while the higher asymmetric mode levels have a negligible contribution.

A more pronounced overpopulation of the highest asymmetric mode levels, and thus dissociation from these levels, would further increase the energy efficiency. This overpopulation can in principle be achieved at lower gas temperature, because this reduces the VT relaxation. On the other hand, it also results in lower dissociation rates of the CO_2 vibrational levels upon collision with O atoms or neutral molecules M. Thus, our calculations reveal that lowering the gas temperature has in general no positive effect on the CO_2 conversion and energy efficiency. Only at 200 L/min and SEI values above 0.7 eV/molec, a gas temperature of 500 K yielded better results than higher temperatures, because the dissociation mainly occurs from the highest asymmetric mode vibrational levels. However, this energy efficient dissociation mechanism cannot compensate for the large amount of power needed to induce it (>9.4 kW) and the maximum energy efficiency obtained is still limited to 25%, although the conversion is slightly enhanced.

Furthermore, our calculations reveal that the recombination reaction (CO + O_2 => CO_2 + O) is the main factor limiting the overall CO_2 conversion, since a large fraction of the dissociated CO_2 (into CO, O and O_2) will recombine again into CO_2. Therefore, we also

performed simulations by removing the O_2 molecules from the system. However, this has only a minor positive effect on the conversion and energy efficiency, since the O atom production through this process, and through the dissociation of O_2, is also inhibited, and these O atoms are needed to react with vibrationally excited CO_2 molecules, to provide more dissociation.

It is clear that the chemistry of CO_2 dissociation in a GAP is quite complicated, and simply reducing the gas temperature or removing the O_2 molecules from the system does not yield significantly better results than the ones obtained already experimentally. We believe that, in order to further improve the performance of the GAP, we should target a higher fraction of gas that can be converted by the plasma column, because the latter is now limited to about 15 %. This effect cannot be studied by 0D modeling, and we would need 3D fluid dynamics simulations for this purpose [23,24,38]. Finally, also mixing the CO_2 gas with a hydrogen source, such as H_2 or CH_4, might improve the CO_2 conversion, as the H atoms can contribute to the CO_2 dissociation. This will be investigated in our future research.

5. Description of Supporting Information

The Supporting Information contains a more detailed description of the 0D model, together with an explanation of the notation of the different vibrational levels implemented in the chemistry set. Moreover, calculated vibrational distribution functions at different positions in the arc column are shown for a plasma power of 650 W and a flow rate of 10 L/min and 22 L/min. Also, the effect of flow rate on the CO_2 conversion and energy efficiency for a maximum gas temperature of 500 K and 3500 K at different SEI values are plotted. Finally, the contribution of the different vibrational levels towards CO_2 dissociation for different conditions is shown.

6. Acknowledgements

The authors acknowledge financial support from the Fund for Scientific Research – Flanders (FWO; Grant no. G.0383.16N) and the IAP/7 (Inter-university Attraction Pole) program 'PSI-Physical Chemistry of Plasma-Surface Interactions' by the Belgian Federal Office for Science Policy (BELSPO). The calculations were performed using the Turing HPC infrastructure at the CalcUA core facility of the Universiteit Antwerpen, a division of the Flemish Supercomputer Center VSC, funded by the Hercules Foundation, the Flemish Government (department EWI) and the Universiteit Antwerpen. Finally, the authors would like to thank Marleen Ramakers and Georgi Trenchev for providing the experimental data and the 3D fluid modelling results as input data for the model, respectively.

7. Bibliography

(1) Blunden, J.; Arndt, D. S. State of the Climate in 2015. *Bull. Amer. Meteor. Soc.* **2016**, *97* (8), S1–S275.

(2) UNFCCC. *Report of the Conference of the Parties on Its Twenty-First Session, Held in Paris from 30 November to 13 December 2015*; 2015.

(3) McDonough, W.; Braungart, M.; Anastas, P. T.; Zimmerman, J. B. Peer Reviewed: Applying the Principles of Green Engineering to Cradle-to-Cradle Design. *Environ. Sci. Technol.* **2003**, *37* (23), 434A–441A.

(4) Snoeckx, R.; Bogaerts, A. Plasma Technology - a Novel Solution for CO_2 Conversion? *Chem. Soc. Rev.* **2017**, in press, DOI: 10.1039/C6CS00066E.

(5) Aerts, R.; Somers, W.; Bogaerts, A. Carbon Dioxide Splitting in a Dielectric Barrier Discharge Plasma: A Combined Experimental and Computational Study. *ChemSusChem* **2015**, *8* (4), 702–

716.

(6) Ozkan, A.; Dufour, T.; Silva, T.; Britun, N.; Snyders, R.; Reniers, F.; Bogaerts, A. DBD in Burst Mode : Solution for More Efficient CO_2 Conversion ? *Plasma Sources Sci. Technol.* **2016**, *25* (5), 55005.

(7) Paulussen, S.; Verheyde, B.; Tu, X.; De Bie, C.; Martens, T.; Petrovic, D.; Bogaerts, A.; Sels, B. Conversion of Carbon Dioxide to Value-Added Chemicals in Atmospheric Pressure Dielectric Barrier Discharges. *Plasma Sources Sci. Technol.* **2010**, *19*, 34015.

(8) Silva, T.; Britun, N.; Godfroid, T.; Snyders, R. Optical Characterization of a Microwave Pulsed Discharge Used for Dissociation of CO_2. *Plasma Sources Sci. Technol.* **2014**, *23*, 25009.

(9) Kwak, H. S.; Uhm, H. S.; Hong, Y. C.; Choi, E. H. Disintegration of Carbon Dioxide Molecules in a Microwave Plasma Torch. *Sci. Rep.* **2015**, *5*, 18436.

(10) van Rooij, G. J.; van den Bekerom, D. C. M.; den Harder, N.; Minea, T.; Berden, G.; Bongers, W. A.; Engeln, R.; Graswinckel, M. F.; Zoethout, E.; van de Sanden, M. C. M. Taming Microwave Plasma to Beat Thermodynamics in CO_2 Dissociation. *Faraday Discuss.* **2015**, *183*, 233–248.

(11) Kozák, T.; Bogaerts, A. Splitting of CO_2 by Vibrational Excitation in Non-Equilibrium Plasmas: A Reaction Kinetics Model. *Plasma Sources Sci. Technol.* **2014**, *23*, 45004.

(12) Kozak, T.; Bogaerts, A. Evaluation of the Energy Efficiency of CO_2 Conversion in Microwave Discharges Using a Reaction Kinetics Model. *Plasma Sources Sci. Technol.* **2015**, *24*, 15024.

(13) Asisov, R. I.; Givotov, V. K.; Krasheninnikov, E. G.; Potapkin, B. V.; Rusanov, V. D.; Fridman, A. Carbon Dioxide Dissociation in Non-Equilibrim Plasma. *Sov. Phys. Dokl.* **1983**, *271*, 94.

(14) Bongers, W.; Bouwmeester, H.; Wolf, B.; Peeters, F.; Welzel, S.; van den Bekerom, D.; den

Harder, N.; Goede, A.; Graswinckel, M.; Groen, P. W.; et al. Plasma-Driven Dissociation of CO_2 for Fuel Synthesis. *Plasma Process. Polym.* **2016**, *14*, e1600126.

(15) Berthelot, A.; Bogaerts, A. Modeling of CO_2 Splitting in a Microwave Plasma: How to Improve the Conversion and Energy Efficiency. *J. Phys. Chem. C* **2017**, *121* (15), 8236–8251.

(16) Fridman, A. *Plasma Chemistry*; Cambridge University Press: New York, U.S.A., 2008.

(17) Spencer, L. F.; Gallimore, A. D. Efficiency of CO_2 Dissociation in a Radio-Frequency Discharge. *Plasma Chem. Plasma Process.* **2011**, *31* (1), 79–89.

(18) Indarto, A.; Yang, D. R.; Choi, J. W.; Lee, H.; Song, H. K. Gliding Arc Plasma Processing of CO_2 Conversion. *J. Hazard. Mater.* **2007**, *146*, 309–315.

(19) Indarto, A.; Choi, J.; Lee, H.; Song, H. K. Conversion of CO_2 by Gliding Arc Plasma. *Environ. Eng. Sci.* **2012**, *23* (6), 1033–1043.

(20) Sun, S. R.; Wang, H. X.; Mei, D. H.; Tu, X.; Bogaerts, A. CO_2 Conversion in a Gliding Arc Plasma: Performance Improvement Based on Chemical Reaction Modeling. *J. CO2 Util.* **2016**, *17*, 220–234.

(21) Nunnally, T.; Gutsol, K.; Rabinovich, A.; Fridman, A.; Gutsol, A.; Kemoun, A. Dissociation of CO_2 in a Low Current Gliding Arc Plasmatron. *J. Phys. D. Appl. Phys.* **2011**, *44*, 274009.

(22) Nunnally, T. P. Application of Low Current Gliding Arc Plasma Discharges for Hydrogen Sulfide Decomposition and Carbon Dioxide Emission Reduction, PhD Dissertation, Drexel University, PhD Thesis, Drexel University, 2011.

(23) Ramakers, M.; Trenchev, G.; Heijkers, S.; Wang, W.; Bogaerts, A. Gliding Arc Plasmatron: Providing a Novel Method for Carbon Dioxide Conversion. *Chem. Sus. Chem.* **2017**, *10*, 2642–2652.

(24) Trenchev, G.; Kolev, S.; Wang, W.; Ramakers, M.; Bogaerts, A. CO_2 Conversion in a Gliding Arc Plasmatron : Multi- Dimensional Modelling for Improved Efficiency. *J.CO2 Util.* submitted.

(25) Liu, J. L.; Park, H. W.; Chung, W. J.; Park, D. W. High-Efficient Conversion of CO_2 in AC-Pulsed Tornado Gliding Arc Plasma. *Plasma Chem. Plasma Process.* **2016**, *36* (2), 437–449.

(26) Zhang, J. Q.; Yang, Y. J.; Zhang, J. S.; Liu, Q. Study on the Conversion of CH_4 and CO_2 Using a Pulsed Microwave Plasma under Atmospheric Pressure. *Acta Chim. Sin.* **2002**, *60* (96), 1973–1980.

(27) De Bie, C.; Martens, T.; van Dijk, J.; Paulussen, S.; Verheyde, B.; Corthals, S.; Bogaerts, A. Dielectric Barrier Discharges Used for the Conversion of Greenhouse Gases: Modeling the Plasma Chemistry by Fluid Simulations. *Plasma Sources Sci. Technol.* **2011**, *20* (2), 24008.

(28) Tu, X.; Gallon, H. J.; Twigg, M. V; Gorry, P. A.; Whitehead, J. C. Dry Reforming of Methane over a Ni / Al_2O_3 Catalyst in a Coaxial Dielectric Barrier Discharge Reactor. *J. Phys. D Appl. Phys.* **2011**, *44*, 274007.

(29) Wang, Q.; Yan, B. H.; Jin, Y.; Cheng, Y. Dry Reforming of Methane in a Dielectric Barrier Discharge Reactor with Ni/Al_2O_3 Catalyst: Interaction of Catalyst and Plasma. *Plasma Chem. Plasma Process.* **2009**, *29* (18), 217–228.

(30) Snoeckx, R.; Aerts, R.; Tu, X.; Bogaerts, A. Plasma-Based Dry Reforming: A Computational Study Ranging from the Nanoseconds to Seconds Time Scale. *J. Phys. Chem. C* **2013**, *117*, 4957–4970.

(31) Gallon, H. J.; Tu, X.; Whitehead, J. C. Effects of Reactor Packing Materials on H_2 Production by CO_2 Reforming of CH_4 in a Dielectric Barrier Discharge. *Plasma Process. Polym.* **2012**, *9* (1), 90–97.

(32) Snoeckx, R.; Ozkan, A.; Reniers, F.; Bogaerts, A. The Quest for Value-Added Products from

Carbon Dioxide and Water in a Dielectric Barrier Discharge: A Chemical Kinetics Study. *ChemSusChem* **2017**, *10* (2), 409–424.

(33) Snoeckx, R.; Heijkers, S.; Van Wesenbeeck, K.; Lenaerts, S.; Bogaerts, A. CO_2 Conversion in a Dielectric Barrier Discharge Plasma: N_2 in the Mix as a Helping Hand or Problematic Impurity? *Energy Environ. Sci.* **2016**, *9*, 30–39.

(34) Heijkers, S.; Snoeckx, R.; Kozak, T.; Silva, T.; Godfroid, T.; Britun, N.; Snyders, R.; Bogaerts, A. CO_2 Conversion in a Microwave Plasma Reactor in the Presence of N_2 : Elucidating the Role of Vibrational Levels. *J. Phys. Chem. C* **2015**, *119*, 12815–12828.

(35) Kano, M.; Satoh, G.; Iizuka, S. Reforming of Carbon Dioxide to Methane and Methanol by Electric Impulse Low-Pressure Discharge with Hydrogen. *Plasma Chem. Plasma Process.* **2012**, *32*, 177–185.

(36) Kogelschatz, U. Dielectric-Barrier Discharges: Their History, Discharge Physics, and Industrial Applications. *Plasma Chem. Plasma Process.* **2003**, *23* (1), 1–46.

(37) Kalra, C. S.; Cho, Y. I.; Gutsol, A.; Fridman, A.; Rufael, T. S. Gliding Arc in Tornado Using a Reverse Vortex Flow. *Rev. Sci. Instrum.* **2005**, *76* (2), 25110.

(38) Trenchev, G.; Kolev, S.; Bogaerts, A. A 3D Model of a Reverse Vortex Flow Gliding Arc Reactor. *Plasma Sources Sci. Technol.* **2016**, *25* (3), 35014.

(39) Koelman, P.; Heijkers, S.; Tadayon Mousavi, S.; Graef, W.; Mihailova, D.; Kozak, T.; Bogaerts, A.; van Dijk, J. A Comprehensive Chemical Model for the Splitting of CO_2 in Non-Equilibrium Plasmas. *Plasma Process. Polym.* **2016**, *14*, 1600185.

(40) Phelps, A. V. Phelps Database www.lxcat.net.

(41) Lowke, J. J.; Phelps, A. V.; Irwin, B. W. Predicted Electron Transport Coefficients and

Operating Characteristics of CO_2/N_2/He Laser Mixtures. *J. Appl. Phys.* **1973**, *44* (10), 4664–4671.

(42) Hake, R. D.; Phelps, A. V. Momentum-Transfer and Inelastic-Collision Cross Sections for Electrons in O_2, CO, and CO_2. *Phys. Rev.* **1967**, *158* (1), 70–84.

(43) Grofulovic, M.; Alves, L. L.; Guerra, V. Electron-Neutral Scattering Cross Sections for CO_2 a Complete and Consistent Set and an Assessment of Dissociation. *J. Phys. D Appl. Phys.* **2016**, *49*, 395207.

(44) Bogaerts, A.; Wang, W.; Berthelot, A.; Guerra, V. Modeling Plasma-Based CO_2 Conversion : Crucial Role of the Dissociation Cross Section. *Plasma Sources Sci. Technol.* **2016**, *25*, 55016.

(45) Pietanza, L. D.; Colonna, G.; D'Ammando, G.; Laricchiuta, A.; Capitelli, M. Vibrational Excitation and Dissociation Mechanisms of CO_2 under Non-Equilibrium Discharge and Post-Discharge Conditions. *Plasma Sources Sci. Technol.* **2015**, *24* (4), 42002.

(46) Pietanza, L. D.; Colonna, G.; D'Ammando, G.; Laricchiuta, A.; Capitelli, M. Electron Energy Distribution Functions and Fractional Power Transfer In "cold" and Excited CO_2 Discharge and Post Discharge Conditions. *Phys. Plasmas* **2016**, *23* (1), 13515.

(47) Pietanza, L. D.; Colonna, G.; D'Ammando, G.; Laricchiuta, A.; Capitelli, M. Non Equilibrium Vibrational Assisted Dissociation and Ionization Mechanisms in Cold CO_2 Plasmas. *Chem. Phys.* **2016**, *468*, 44–52.

(48) Snoeckx, R.; Setareh, M.; Aerts, R.; Simon, P.; Maghari, A.; Bogaerts, A. Influence of N_2 Concentration in a CH_4/N_2 Dielectric Barrier Discharge Used for CH_4 Conversion into H_2. *Int. J. Hydrogen Energy* **2013**, *38* (36), 16098–16120.

(49) Menter, F. R.; Kuntz, M.; Langtry, R. Ten Years of Industrial Experience with the SST Turbulence Model. *Turbul. Heat Mass Transf.* **2003**, *4*, 625–632.

(50) Czernichowski, A.; Fridman, A. A.; Simek, M.; Musiol, K.; Pawelec, E.; Dittrichova, L. Spectral and Electrical Diagnostics of Gliding Arc. *Acta Phys. Pol. A* **1996**, *89* (5), 595–603.

(51) Goede, A. P. H.; Bongers, W. a; Graswinckel, M. G.; Sanden, R. M. C. . Van De; Martina, L.; Jochen, K.; Schulz, A.; Mathias, W. Production of Solar Fuels by CO_2 Plasmolysis. *3rd Eur. Energy Conf. Budapest* **2014**, *79*, 1005.

(52) Chernets, I.; Nirenberg, G.; Fridman, A.; Rabinovich, A. Development of High-Power Plasma Reformer and Power Supply for Large Scale Applications. *Proc. 20th Int. Symp. Plasma Chem. Philadelphia, Pennsylvania* **2011**.

(53) Givotov, V. K.; Fridman, A. A.; Krotov, M. F.; Krasheninnikov, E. G.; Patrushev, B. I.; Rusanov, V. D.; Sholin, G. V. Plasmochemical Methods of Hydrogen Production. *Int. J. Hydrog. Energy* **1981**, *6* (5), 441–449.

(54) Aerts, R.; Snoeckx, R.; Bogaerts, A. In-Situ Chemical Trapping of Oxygen in the Splitting of Carbon Dioxide by Plasma. *Plasma Process. Polym.* **2014**, 985–992.

8.0 TOC Graphic

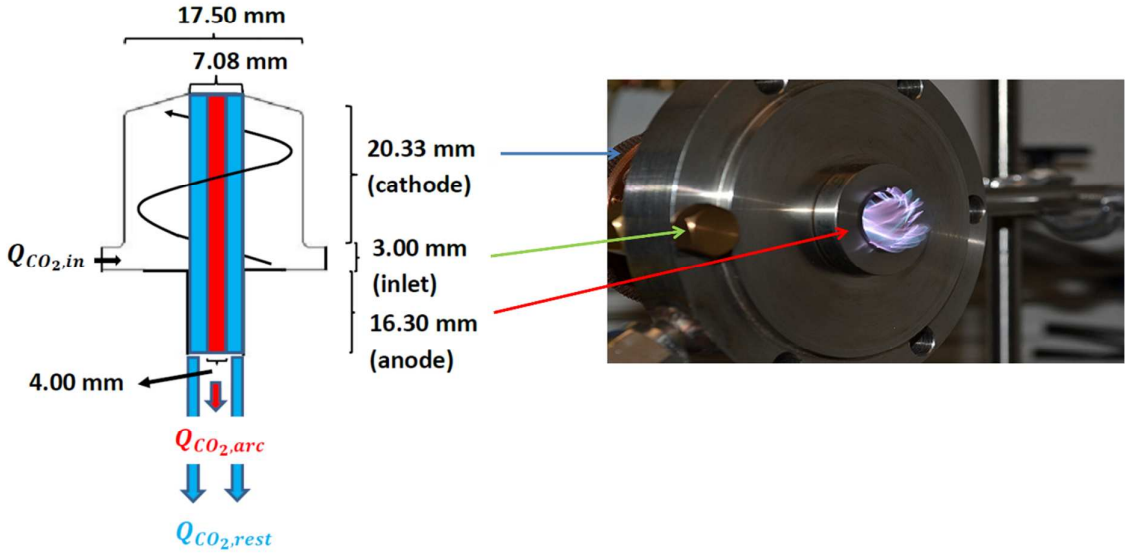
17.50 mm
7.08 mm
20.33 mm
(cathode)
3.00 mm
(inlet)
16.30 mm
(anode)
$Q_{CO_2,in}$
4.00 mm
$Q_{CO_2,arc}$
$Q_{CO_2,rest}$